Accessing the Temperature of the Quark-Gluon Plasma at Different Stages

In a Quark-Gluon Plasma (QGP) [1,2], the fundamental building blocks of matter can be found at the most extreme temperature and density [3,4] conditions. It is believed to have existed in the early stages of the Universe [5–7], in supernova explosions [8], and in the core of neutron stars [9,10]. Ultra-relativistic heavy-ion collisions, in which quarks and gluons are liberated from confinement within nucleons, can recreate a QGP. The thermodynamic and hydrodynamic properties of the QGP, such as temperature, baryon chemical potential, and viscosity, have been under intense theoretical investigations in lattice Quantum Chromodynamics (QCD) calculations [11,12] and in experiments utilizing the world's most powerful supercomputers and particle accelerators, respectively [13,14]. Thermal lepton pairs (e^+e^- and $\mu^+\mu^-$) from QGP radiation are ideal, penetrating probes of the true temperature of the emitting source, since they do not suffer from strong final state interactions nor from blue-shift effects through the collective motion of the rapidly expanding system [15–17]. The invariant mass spectra of thermal e^+e^- pairs over a large kinematic range and different beam energies at the Relativistic Heavy Ion Collider (RHIC) have been studied. We extract from intermediate invariant mass pairs the temperature of the QGP radiation averaged over the early space-time evolution. From low-mass pairs, which are dominated by the decays from in-medium ρ^0 vector mesons, we extract the temperature averaged over the later stage of the evolution. The average temperature from the low-mass region is measured to be $(1.90 \pm 0.20) \times 10^{12}$ Kelvin. It is close to the chemical freeze-out temperature derived

in the Statistical Hadronization Model [18] and the transition temperature from lattice QCD calculations [11,12]. The temperature from intermediate mass pairs is significantly higher, and averaged to be $(3.72 \pm 0.49) \times 10^{12}$ Kelvin. These measurements provide direct experimental access to the QGP temperature and deliver the experimental evidence that the ρ^0 hadron undergoes a significant in-medium broadening effects when it is produced around the phase boundary between QGP and hadronic matter.

1 Introduction

The state of QCD matter is typically characterized by its temperature and baryon chemical potential as depicted in Fig. 1. The baryon chemical potential μ_B, a measure of the free energy change due to the increase of baryon number in a fixed volume in the system, can be extracted from yields among many hadrons at given beam energy in the heavy-ion collisions [11–14]. Dielectrons, typically defined as e^+e^- pairs, are excellent thermometers of the extremely hot and dense QCD matter [19] created in high energy heavy-ion collisions. Electrons are members of a class of fundamental particles called leptons that do not undergo strong interactions. Consequently, they have minimal interactions with the predominantly strongly-interacting particles throughout the evolution of the system in both its initial quark-gluon and the final hadronic state. Similar to other blackbody radiation processes, the higher the temperature, the harder the dielectron energy and mass spectra. In a collision where the system cools as it expands, different ranges of the dielectron energy and spectra would be dominated by the radiation at the different stages of the evolution. QGP bulk matter consists of thermalized quarks and gluons under the most extreme conditions and its temperature can reach

a few hundreds of MeV, where 100 MeV = 1.16×10^{12} K. It radiates both photons and lepton pairs which can be harvested by experiments as thermometer [1,20,21]. Photons have been used to measure the QGP temperature at the Relativistic Heavy Ion Collider (RHIC) and the Large Hadron Collider (LHC) in the last two decades [22–25]. However, heavy-ion collisions at these ultra-relativistic energies result in a rapid bulk expansion with a complicated flow profile. The local flow velocity is a significant fraction of the speed of light and alters the energy spectrum of photons. This blue-shift effect makes the extraction of a true "blackbody" radiation temperature from the detected photon energy spectrum very complex, if not impossible, and overly reliant on model assumptions [17]. On the contrary, electron pairs from the thermal emission provide an additional degree of freedom for the reconstruction of a Lorentz-invariant quantity: its invariant mass [15,16]. The invariant mass spectrum of thermal dielectrons, by definition, is immune to the blue-shift effect and is therefore able to provide a true measurement of the temperature of the QGP at different stages of the evolution. At the early stage of the QGP evolution, thermal dielectrons are predicted to be dominantly produced via the annihilation among quarks, anti-quarks and gluons. When the system cools down, the liberated quarks and gluons begin the hadranization process into baryons and mesons at the phase transition. The resulting strongly-interacting partonic and hadronic mixed medium still exhibits certain bulk thermodynamic and hydrodynamic properties and continues to expand and cool down. At this stage and later on, the dielectrons are mostly from the decays of ρ^0 vector meson produced inside the medium. The dense hadronic medium continuously creates ρ^0 through intense hadronic collisions while the vector meson also decays spontaneously with a lifetime of 1 fm/c or less. The collisional and in-medium broadening effects on the ρ^0 spectral

function lead the dielectron spectra to approach a thermal distribution [26–29]. Therefore, the thermal dielectron invariant mass spectra from the decay of the in-medium ρ^0 vector meson are considered as an excellent experimental probe of the dissolving hadronic spectral functions close to the QCD phase boundary.

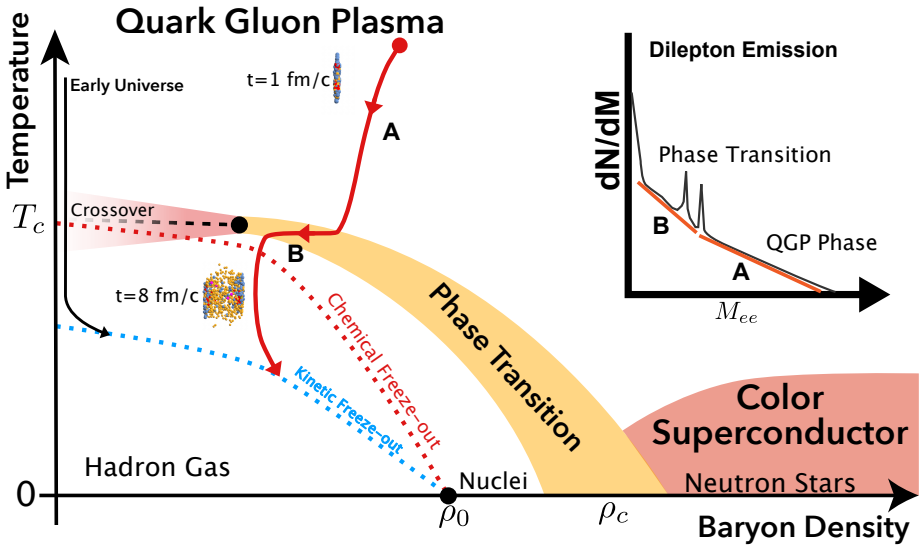

Figure 1: (Color online) **A schematic view of e^+e^- pair production and QCD phase diagram**. The diagram illustrates the matter properties in baryon density (x-axis) and temperature (y-axis) with landmarks of normal nuclear density, neutron stars, and phase transition to QGP. A heavy-ion collision creates the QGP at high density and temperature shortly after the initial impact and the system evolves along the arrow toward phase boundary and hadronization. The insert depicts the dilepton spectrum with low-mass and intermediate-mass ranges corresponding to the dominant emission contribution from the transition and the QGP phases, respectively.

In the past two decades, measurements of the thermal dilepton (e^+e^- and $\mu^+\mu^-$) production in heavy-ion collisions have been an essential scientific program to several experiments conducted

at SIS18 [30,31], Supper Proton Synchrotron (SPS) [32–36], RHIC [37–41] and LHC [42] at a wide range of colliding beam energies. The measured dilepton spectra in the low-mass region at both SPS and RHIC provide strong experimental evidence that the spectral function of the in-medium ρ^0 vector meson is significantly broadened without dropping its pole mass. Furthermore, the effective temperature (T_{eff}), an inverse slope parameter of the dimuon transverse-momentum spectrum, was extracted from NA60 data in In+In collisions at $\sqrt{s_{\rm NN}} = 17.3$ GeV [36]. T_{eff} is measured to increase linearly as a function of the diumum mass up to $M_{\mu^+\mu^-}$ <1 GeV/c^2, and then decrease toward higher mass. This feature is consistent with the expectation that the momentum of the low-mass dimuons from the in-medium ρ^0 decay are shifted toward higher momentum when emitted from the hadronic medium with a large radial flow while the higher mass thermal dimuons are mainly from a partonic medium at an earlier stage of the collision. The HADES experiment recently showed that the dielectron mass spectrum exhibits a near-exponential fall-off in the low-mass region in Au+Au collisions at $\sqrt{s_{\rm NN}} = 2.42$ GeV [31]. The average temperature extracted from this exponential spectrum was determined to be 71.8 $\pm$ 2.1 MeV. Although its kinematic reach is below ρ^0 pole mass, it indicates that the ρ^0 resonance spectrum is significantly altered and that frequent interactions among the baryons in the dense hadronic medium could produce a seemingly thermalized system. These previous measurements and knowledge at lower beam energies provide the necessary baselines for temperature measurements at different stages of the collisions at higher energies.

In this article, we present dielectron spectra in Au+Au collisions at beam energies from $\sqrt{s_{\rm NN}} = 19.6$ to 200 GeV using data collected from the STAR Detector at RHIC from year 2010

to year 2018 including two high-statistic datasets at $\sqrt{s_{\rm NN}}$ =19.6 and 54.4 GeV. The temperature of hot nuclear matter from the thermal dielectrons in the low-mass and intermediate-mass regions are extracted. These results provide access to the thermodynamic properties at both the early stage of the QGP phase as well as the late stage near the phase transition to the hadronic matter.

2 Experiment

The thermal dielectrons in this study are measured with the STAR experiment at RHIC. The most relevant STAR detectors for this study are depicted in Fig. 2 (top panel) with a typical event display from the collisions. The charged particles produced in collisions leave ionization trails inside STAR's Time Projection Chamber (TPC). The curvature of a particle trajectory in the magnetic field is used to derive its rigidity (the momentum p divided by the charge q) and the ionization energy loss (dE/dx) deposited along the track inside the gas of the TPC is used to identify the particle species. This measurement of the dE/dx as a function of the particle rigidity (p/q) is illustrated in Fig. 2 (bottom-left panel). In addition, the velocity (β) and mass [$m^2 = p^2(1/\beta^2 - 1)$] of a charged particle originating from the collision point can be measured by the time-of-flight detector (TOF) surrounding the outer barrel of the TPC. The electrons of interest have the characteristics of the dE/dx relativistic rise and the low electron mass as shown in Fig. 2 (bottom-right panel). This combination of two powerful particle identification tools enables the STAR detector to provide excellent electron identification with a hadronic background rejection power of 1:10000 and better. The excellent electron identification and large fiducial acceptance make such difficult measurement possible. The identified electrons and positrons from the same event are

paired to reconstructed pair mass and transverse momentum. However, more than 99% of these pairs are from random combinations (combinatorial background), which need to be subtracted to obtain the raw inclusive dielectron signals. After correcting for the pair reconstruction efficiency and acceptance, the fully corrected inclusive dielectron signals can be calculated. The black dots in top two panels of Figure. 3 show the fully corrected inclusive dielectron invariant mass spectrum. More details on the measurements can be found in Method section.

The measured dielectrons are accumulative contributions from various stages of the evolution of the heavy-ion collisions. These include dielectrons from the thermal QCD medium of the collision as well as the non-thermal physics sources, commonly referred to as "cocktails". At the initial impact of the collision, dielectrons can be produced through the annihilation of valence quarks and sea anti-quarks between colliding target and projectile nuclei (Drell-Yan process). After the hot medium has disintegrated at the very late stage, the dielectrons can also be produced from the decays of long-lived hadrons (Dalitz decays: π^0, η, $\eta' \rightarrow \gamma e^+e^-$ and $\omega \rightarrow \pi^0 e^+e^-$, $\phi \rightarrow \eta e^+e^-$; two body decays: ω, ϕ, J/$\psi \rightarrow e^+e^-$ or the semi-leptonic decays of open charm hadrons). The contributions from these physics backgrounds can be well determined via the cocktail simulation techniques and are shown as the dashed curves in the top two panels of Fig. 3. The black curves show the sum of all physics background contributions (Cocktail Sum). The fully corrected data exceeds the Cocktail Sum substantially over a large mass region, indicating clear contributions from thermal dielectrons. To quantify the thermal contributions, the excess dielectron mass spectrum are obtained by subtracting the Cocktail Sum from the fully corrected data. Further details about the cocktail simulations can be found in the Method section.

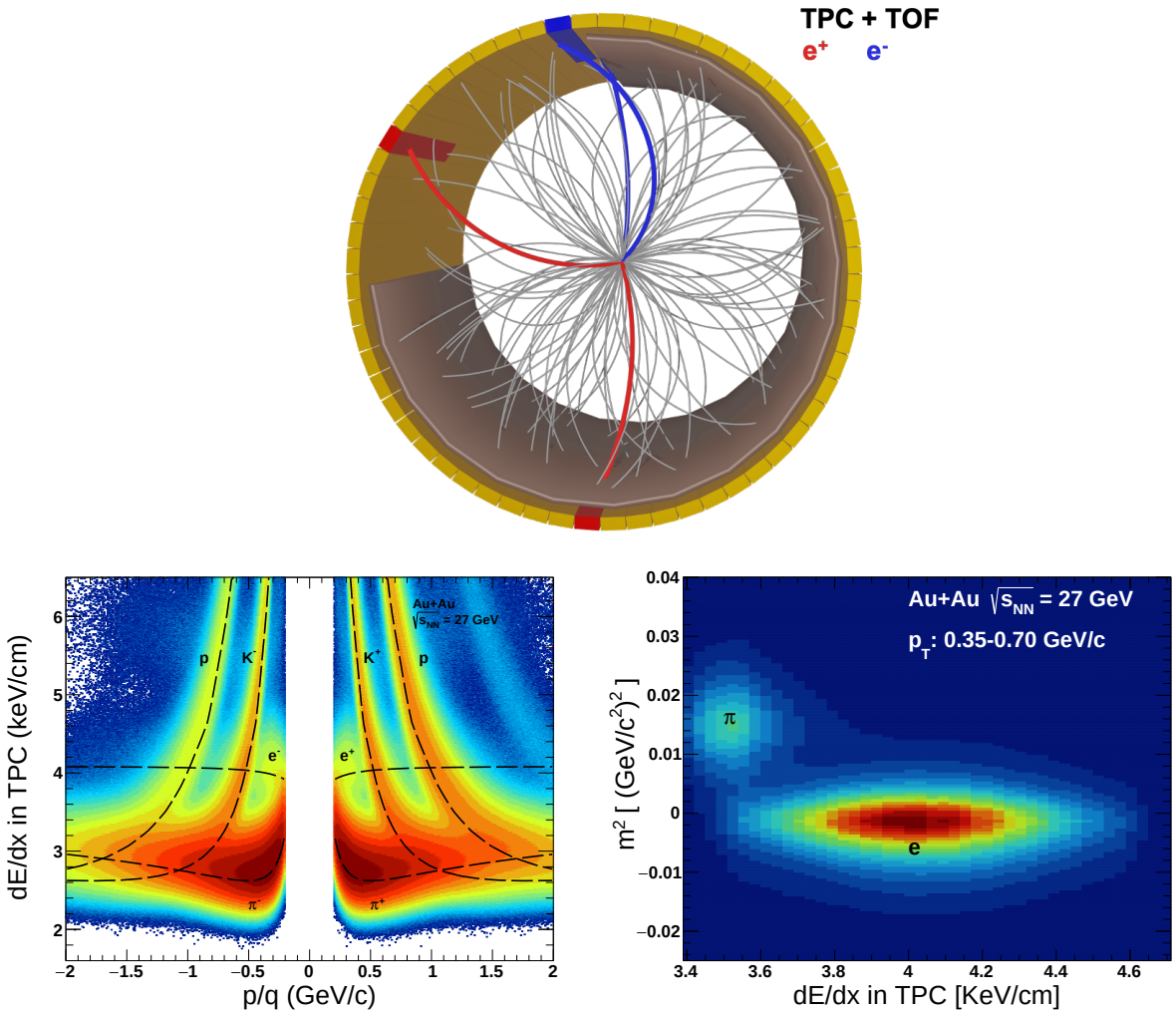

Figure 2: (Color online) **A schematic display of a Au+Au collision reconstructed with the STAR detector.** Top panel shows that charged particles ionize the gas in the STAR TPC, forming three-dimensional tracks (gray lines) that curve under the magnetic field of the detector. As tracks exit the outer radius of TPC, they leave signals (red and blue trays) in the time-of-flight (TOF) detector. Electron (blue lines) and positron (red lines) tracks are identified based on the normalized ionization energy loss (dE/dx) and the mass square (m^2)derived from the velocity (β) by TOF and momentum (p) from TPC . The bottom-left panel shows the dE/dx as a function of momentum and the bottom-right panel shows the m^2 v.s. dE/dx distribution, respectively.

3 Results and Discussions

The measured invariant-mass spectra of the thermal dielectron (excess dielectron) are shown in the bottom two panels of Fig. 3. The spectra are normalized by the charge multiplicity dN_{ch}/dy in order to compare the measurements among different colliding species and beam energies. The left panel of Fig. 3 shows the results in the low-mass region (LMR), and it is observed that the STAR data from both 54.4 GeV and 27 GeV Au+Au collisions are consistent with each other within the entire mass region. Additionally, the STAR data at LMR also show good agreement with the dimuon spectrum from In+In collisions at$\sqrt{s_{\rm NN}}$ = 17.3 GeV while those at IMR at STAR are systematically higher than that at lower energy. This may indicate that the thermal dileptons at LMR from these three measurements are radiated sources with similar temperature and density while there is an indication that the dileptons from IMR are from sources with different temperature. To quantify the temperature of the thermal source responsible for LMR radiation, a function that combines the in-medium resonance structure and the structure-less shape is used to fit the measured mass spectrum. The in-medium resonance shape is described by a relativistic Breit-Wigner function, BW, multiplied by the Boltzmann factor $PS = exp(-M/T)$ to account for the phase space [43,44]. In this function, BW = $MM_0\Gamma/[(M_0^2 - M^2)^2 + M_0^2\Gamma^2]$, M is the invariant mass of the pair, $\Gamma = \Gamma_0 \times (M_0/M) \times [(M^2 - 4m^2)/(M_0^2 - 4m^2)]^{3/2}$ is the width, Γ_0 and M_0 are width and pole mass of ρ^0 meson while the m is the mass of the decayed lepton. If the ρ^0 is completely dissolved inside the medium, its mass structure spreads out and approaches a smooth distribution similar to the the quark-antiquark continuum (QGP thermal radiation) which can be described by $M^{3/2} \times exp(-M/T)$ as pointed out in ref. [16,31]. The extracted temperatures (T_{LMR}) from LMR

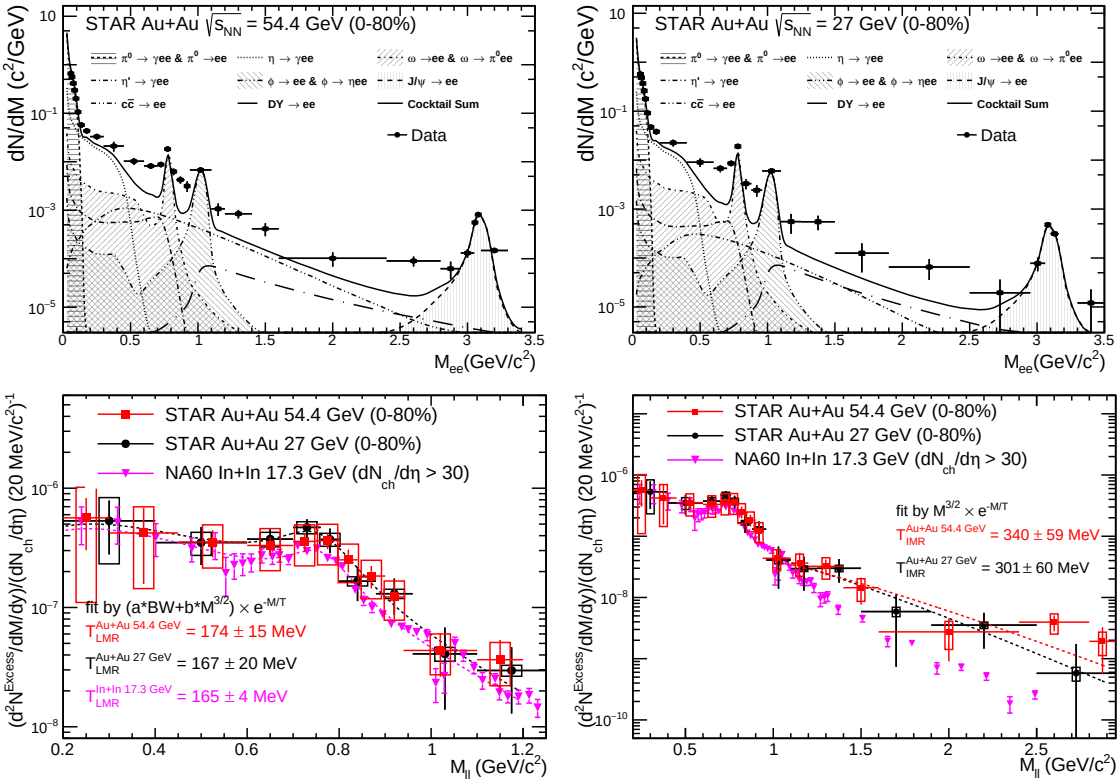

Figure 3: (Color online) **Dielectron invariant mass spectrum.** Top two panels show the fully corrected inclusive dielectron mass spectrum (black dots) compared to the physics background (dashed and shaded lines) in Au+Au collisions at $\sqrt{s_{NN}}$ = 54.4 GeV and 27 GeV. Bottom two panels show the thermal dielectron mass spectrum from 54.4 GeV (red dots) and 27 GeV (black dots) compared to the NA60 thermal dimuon data (blue inverted triangles). Vertical bars and boxes around data points represent the statistical and systematic uncertainties, respectively.

thermal dielectron mass spectrum are 167 ± 20 MeV and 174 ± 15 MeV for the Au+Au collisions at $\sqrt{s_{\rm NN}} = 27$ and 54.4 GeV, respectively. The similar fit to NA60 data gives a temperature of 165 ± 4 MeV. The extracted temperatures from the LMR thermal dileptons of different collision energies and species are consistent with each other, and suggestive that they are radiated from thermal sources with similar temperature. In the intermediate mass region (IMR, $1 < M < 2.9$ GeV/c^2), data between 27 GeV and 54.4 GeV Au+Au collisions are consistent within uncertainty and slightly higher than the data from NA60. The mass spectrum in this mass region is smoothly distributed, and the temperature is extracted using the continuum shape $M^{3/2} \times exp(-M/T)$, as predicted in ref. [16]. The extracted temperatures T_{IMR} for the 27 GeV and 54.4 GeV Au+Au collisions are 301 ± 60 MeV and 340 ± 59 MeV, respectively. When fitting to the thermal dimuon spectra of NA60 data in this mass region, the temperature is 246 ± 15 MeV. These temperatures reflect an average over a certain period of the space-time evolution of the hot medium. The extracted temperature for the low-mass region is significantly lower than that of the intermediate-mass region. This observation is consistent with the expectation that LMR thermal dileptons are emitted at a later stage of the medium evolution around phaser transition while those at the IMR are mainly from the earlier stage with much higher temperature.

Figure. 4 summaries the temperature measured as a function of the baryonic chemical potential. The chemical freeze-out temperature T_{ch} and baryonic chemical potential μ_B can be well determined via analyzing the hadron production yields with the statistical thermal models [18]. The chemical freeze-out temperatures extracted from the statistical thermal models (SH, GCE, SCE) [18,45] are shown as solid dots and open circles in the figure. Theoretical studies of lattice

QCD at the small μ_B predict a crossover type of phase transition with continuous, smooth but rapid increase of thermodynamic quantities in a narrow region around the critical temperature $T_C = 156 \pm 5$ MeV at $\mu_B = 0$. It decreases slightly towards higher μ_B as shown in the green band in the figure. In the meanwhile, we also extracted the temperatures based on the low-mass thermal dielectron spectra published with the STAR BES-I data in Au+Au collisions at different collision energies of $\sqrt{s_{\rm NN}} = 19.6, 37, 62.4, 200$ GeV [38,40]. A temperature was extracted with the continuous shape of $M^{3/2} \times exp(-M/T)$. This simplification was determined by the limited statistics in those measurements and that the resonance structures of the in-medium ρ^0 were removed due to the over-subtraction of ω meson and ϕ meson contributions in that analysis approach [38,40]. Future BES-II data with high statistics may be more sensitive to the different functional forms. The extracted T_{LMR} are shown as open blue squares in the figure, and are in good agreement with the new STAR results from data at collisions beam energies of 27 GeV and 54.4 GeV as well as the result (blue rhombus) extracted from NA60 data. Moreover, all the temperatures are found to stay around the phase transition temperature T_C and the chemical freeze-out temperature T_{ch}.

It has been a long-standing challenge and open issue on the phenomenological observation that the temperature (T_{ch}) extracted from the chemical yields of the final-state hadrons coincides with the QCD phase transition temperature (T_C) from the Lattice QCD [18]. Can the present dilepton measurements provide new insight in resolving such an issue? Stable hadrons emerge from the chemical freeze-out at that instant and their yields are an integration over the whole volume of the system. Therefore, the extracted temperature by definition could not be higher than the hadronization and phase transition temperature. In principle, yields of the low-mass thermal dileptons are

accumulative from the QGP stage to the kinetic freeze-out. Therefore, the yield is an integration over the whole system volume and over the entire evolution time duration. In comparison of the dilepton yields normalized by the total number of charged particles from heavy-ion collisions to the expected yields from the hadronic channel in $p+p$ collisions and from the thermal model predictions, we further found that the dielectron yields is more than a factor of 5 larger than those two baseline yields (see Method and BES-I [38,40]). The high yields of dileptons, the strong in-medium broadening of ρ spectral function and the coincidence of three temperatures (T_C, T_{ch} and T_{LMR}) suggest that the low-mass thermal dileptons be dominantly emitted over a long period of time at high density with a constant temperature. Such scenario is possible if it happens around a phase transition and/or the softest point of an equation of state. This in turn provides a direct experimental tool for accessing the temperature at the vicinity where the deconfinement phase transition occurs - one of the most fundamental landmarks of the QCD phase diagram.

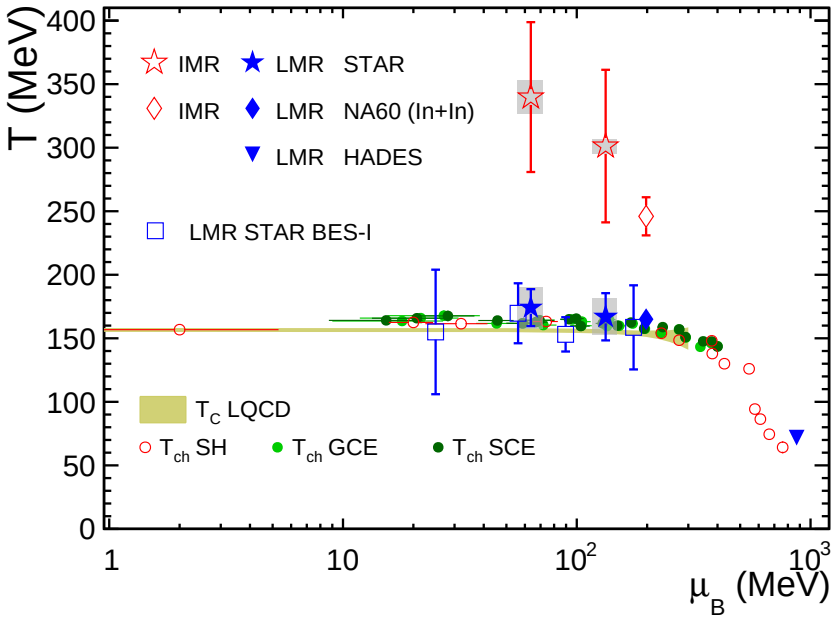

Figure 4: (Color online) **Temperatures vs. baryonic chemical potential.** Temperatures extracted from in-medium ρ; (Blue solid stars) dominant region and QGP (open red stars) dominant region from STAR data are compared to the temperatures extracted from NA60 data (Blue rhombus and open red rhombus) and HADES data (blue invert triangle). Chemical freeze-out temperatures extracted from the statistical thermal models (GCE, SCE, SH) are shown as solid dots and open circles. The QCD critical temperature T_C at finite chemical baryon density predicted by lattice QCD calculations are shown as green band. Vertical bars and shaded boxes around data points represent the statistical and systematic uncertainties, respectively.

4 Summary

In this study, we present the first direct measurements of the temperature of the strongly interacting hot QCD matter created in Au+Au collisions at RHIC via the thermal dielectrons. Our measurements reveal that the extracted temperatures from the low-mass thermal dielectrons are consistently close to the QCD phase transition temperature derived in lattice QCD calculations and the chemical freeze-out temperature deduced from statistical hadronization models. This finding provides the first direct experimental evidence that the in-medium ρ^0 vector meson is predominantly produced around the phase boundary of QCD matter created in heavy-ion collisions at both RHIC and SPS. The temperature extracted from the intermediate mass thermal dielectrons is $(3.72 \pm 0.49) \times 10^{12}$ Kelvin much higher than the phase transition temperature, consistent with the expectation that their dominant emission source is the deconfined QCD matter, the QGP. This work provides important experimental thermodynamic measurements to map the QCD phase diagram and understand the properties of matter under extreme conditions.

5 Acknowledgement

We thank the RHIC Operations Group and RCF at BNL, the NERSC Center at LBNL, and the Open Science Grid consortium for providing resources and support. This work was supported in part by the Office of Nuclear Physics within the U.S. DOE Office of Science, the U.S. National Science Foundation, the Ministry of Education and Science of the Russian Federation, National Natural Science Foundation of China, Chinese Academy of Science, the Ministry of Science and

Technology of China and the Chinese Ministry of Education, the National Research Foundation of Korea, Czech Science Foundation and Ministry of Education, Youth and Sports of the Czech Republic, Department of Atomic Energy and Department of Science and Technology of the Government of India, the National Science Centre of Poland, the Ministry of Science, Education and Sports of the Republic of Croatia, RosAtom of Russia and German Bundesministerium fur Bildung, Wissenschaft, Forschung and Technologie (BMBF) and the Helmholtz Association.

1. Shuryak, E. V. Quark-Gluon Plasma and Hadronic Production of Leptons, Photons and Psions. *Phys. Lett. B* **78**, 150 (1978).

2. Gross, D. J., Pisarski, R. D. & Yaffe, L. G. QCD and Instantons at Finite Temperature. *Rev. Mod. Phys.* **53**, 43 (1981).

3. Linde, A. D. Phase Transitions in Gauge Theories and Cosmology. *Rept. Prog. Phys.* **42**, 389 (1979).

4. Roberts, C. D. & Schmidt, S. M. Dyson-Schwinger equations: Density, temperature and continuum strong QCD. *Prog. Part. Nucl. Phys.* **45**, S1–S103 (2000). `nucl-th/0005064`.

5. Olive, K. A. The Quark - hadron transition in cosmology and astrophysics. *Science* **251**, 1194–1199 (1991).

6. Schwarz, D. J. The first second of the universe. *Annalen Phys.* **12**, 220–270 (2003). `astro-ph/0303574`.

7. Boyanovsky, D., de Vega, H. J. & Schwarz, D. J. Phase transitions in the early and the present universe. *Ann. Rev. Nucl. Part. Sci.* **56**, 441–500 (2006). hep-ph/0602002.

8. Fischer, T. *et al.* Quark deconfinement as a supernova explosion engine for massive blue supergiant stars. *Nature Astron.* **2**, 980–986 (2018). 1712.08788.

9. Baym, G. *et al.* From hadrons to quarks in neutron stars: a review. *Rept. Prog. Phys.* **81**, 056902 (2018). 1707.04966.

10. Annala, E., Gorda, T., Kurkela, A., Nättilä, J. & Vuorinen, A. Evidence for quark-matter cores in massive neutron stars. *Nature Phys.* **16**, 907–910 (2020). 1903.09121.

11. Bazavov, A. *et al.* Chiral crossover in QCD at zero and non-zero chemical potentials. *Phys. Lett. B* **795**, 15–21 (2019). 1812.08235.

12. Borsanyi, S. *et al.* QCD Crossover at Finite Chemical Potential from Lattice Simulations. *Phys. Rev. Lett.* **125**, 052001 (2020). 2002.02821.

13. Braun-Munzinger, P., Koch, V., Schäfer, T. & Stachel, J. Properties of hot and dense matter from relativistic heavy ion collisions. *Phys. Rept.* **621**, 76–126 (2016). 1510.00442.

14. Busza, W., Rajagopal, K. & van der Schee, W. Heavy Ion Collisions: The Big Picture, and the Big Questions. *Ann. Rev. Nucl. Part. Sci.* **68**, 339–376 (2018). 1802.04801.

15. van Hees, H. & Rapp, R. Comprehensive interpretation of thermal dileptons at the SPS. *Phys. Rev. Lett.* **97**, 102301 (2006). hep-ph/0603084.

16. Rapp, R. & van Hees, H. Thermal Dileptons as Fireball Thermometer and Chronometer. *Phys. Lett. B* **753**, 586–590 (2016). 1411.4612.

17. Shen, C., Heinz, U. W., Paquet, J.-F. & Gale, C. Thermal photons as a quark-gluon plasma thermometer reexamined. *Phys. Rev. C* **89**, 044910 (2014). 1308.2440.

18. Andronic, A., Braun-Munzinger, P., Redlich, K. & Stachel, J. Decoding the phase structure of QCD via particle production at high energy. *Nature* **561**, 321–330 (2018). 1710.09425.

19. Stoecker, H. & Greiner, W. High-Energy Heavy Ion Collisions: Probing the Equation of State of Highly Excited Hadronic Matter. *Phys. Rept.* **137**, 277–392 (1986).

20. McLerran, L. D. & Toimela, T. Photon and Dilepton Emission from the Quark - Gluon Plasma: Some General Considerations. *Phys. Rev. D* **31**, 545 (1985).

21. Shuryak, E. V. & Xiong, L. Dilepton and photon production in the 'hot glue' scenario. *Phys. Rev. Lett.* **70**, 2241–2244 (1993). hep-ph/9301218.

22. Adare, A. *et al.* Centrality dependence of low-momentum direct-photon production in Au+Au collisions at $\sqrt{s_{NN}} = 200$ GeV. *Phys. Rev. C* **91**, 064904 (2015). 1405.3940.

23. Adam, J. *et al.* Direct photon production in Pb–Pb collisions at $\sqrt{s_{NN}} = 2.76$ TeV. *Physics Letters B* **754**, 235–248 (2016).

24. Acharya, U. A. *et al.* Nonprompt direct-photon production in Au+Au collisions at $\sqrt{s_{NN}} =$ 200 GeV (2022). 2203.17187.

280 25. Acharya, U. A. *et al.* Low-p_T direct-photon production in Au+Au collisions at $\sqrt{s_{NN}} = 39$
281 and 62.4 GeV (2022). 2203.12354.

282 26. Cassing, W., Bratkovskaya, E. L., Rapp, R. & Wambach, J. Probing the rho spectral
283 function in hot and dense nuclear matter by dileptons. *Phys. Rev. C* **57**, 916–921 (1998).
284 nucl-th/9708020.

285 27. Cassing, W. & Bratkovskaya, E. L. Hadronic and electromagnetic probes of hot and dense
286 nuclear matter. *Phys. Rept.* **308**, 65–233 (1999).

287 28. Rapp, R. & Wambach, J. Chiral symmetry restoration and dileptons in relativistic heavy ion
288 collisions. *Adv. Nucl. Phys.* **25**, 1 (2000). hep-ph/9909229.

289 29. Rapp, R. Signatures of thermal dilepton radiation at RHIC. *Phys. Rev. C* **63**, 054907 (2001).
290 hep-ph/0010101.

291 30. Agakichiev, G. *et al.* Dielectron production in C-12+C-12 collisions at 2-AGeV with HADES.
292 *Phys. Rev. Lett.* **98**, 052302 (2007). nucl-ex/0608031.

293 31. Adamczewski-Musch, J. *et al.* Probing dense baryon-rich matter with virtual photons. *Nature*
294 *Phys.* **15**, 1040–1045 (2019).

295 32. Adamova, D. *et al.* Enhanced production of low mass electron pairs in 40-AGeV Pb - Au
296 collisions at the CERN SPS. *Phys. Rev. Lett.* **91**, 042301 (2003). nucl-ex/0209024.

297 33. Agakichiev, G. *et al.* e+ e- pair production in Pb - Au collisions at 158-GeV per nucleon. *Eur.*
298 *Phys. J. C* **41**, 475–513 (2005). nucl-ex/0506002.

299 34. Arnaldi, R. *et al.* Evidence for radial flow of thermal dileptons in high-energy nuclear colli-
300 sions. *Phys. Rev. Lett.* **100**, 022302 (2008). 0711.1816.

301 35. Arnaldi, R. *et al.* First measurement of the rho spectral function in high-energy nuclear colli-
302 sions. *Phys. Rev. Lett.* **96**, 162302 (2006). nucl-ex/0605007.

303 36. Arnaldi, R. *et al.* Evidence for the production of thermal-like muon pairs with masses above
304 1-GeV/c**2 in 158-A-GeV Indium-Indium Collisions. *Eur. Phys. J. C* **59**, 607–623 (2009).
305 0810.3204.

306 37. Adamczyk, L. *et al.* Dielectron Mass Spectra from Au+Au Collisions at $\sqrt{s_{\rm NN}}$ = 200 GeV.
307 *Phys. Rev. Lett.* **113**, 022301 (2014). [Addendum: Phys.Rev.Lett. 113, 049903 (2014)],
308 1312.7397.

309 38. Adamczyk, L. *et al.* Energy dependence of acceptance-corrected dielectron excess mass spec-
310 trum at mid-rapidity in Au+Au collisions at $\sqrt{s_{NN}} = 19.6$ and 200 GeV. *Phys. Lett. B* **750**,
311 64–71 (2015). 1501.05341.

312 39. Adamczyk, L. *et al.* Measurements of Dielectron Production in Au+Au Collisions at $\sqrt{s_{\rm NN}}$ =
313 200 GeV from the STAR Experiment. *Phys. Rev. C* **92**, 024912 (2015). 1504.01317.

314 40. Adam, J. *et al.* Measurements of Dielectron Production in Au+Au Collisions at $\sqrt{s_{NN}}$= 27,
315 39, and 62.4 GeV from the STAR Experiment (2018). 1810.10159.

316 41. Adare, A. *et al.* Dielectron production in Au+Au collisions at $\sqrt{s_{NN}}$=200 GeV. *Phys. Rev. C*
317 **93**, 014904 (2016). 1509.04667.

318 42. Acharya, S. *et al.* Measurement of dielectron production in central Pb-Pb collisions at $\sqrt{s_{\mathrm{NN}}}$
319 = 2.76 TeV. *Phys. Rev. C* **99**, 024002 (2019). 1807.00923.

320 43. Shuryak, E. V. & Brown, G. E. Matter induced modification of resonances at RHIC freezeout.
321 *Nucl. Phys. A* **717**, 322–335 (2003). hep-ph/0211119.

322 44. Adams, J. *et al.* Rho0 production and possible modification in Au+Au and p+p collisions at
323 S(NN)**1/2 = 200-GeV. *Phys. Rev. Lett.* **92**, 092301 (2004). nucl-ex/0307023.

324 45. Adamczyk, L. *et al.* Bulk Properties of the Medium Produced in Relativistic Heavy-Ion Colli-
325 sions from the Beam Energy Scan Program. *Phys. Rev. C* **96**, 044904 (2017). 1701.07065.